10 IMAGING SYSTEMS AND APPLICATIONS

Chapter Contents

10.1   INTRODUCTION

The modern diagnostic imaging system is continuing to evolve and, as a result, is becoming more complicated with new modes and features. System functions are the last blocks added to the overall block diagram (see Figure 2.14). This chapter introduces the basic principles of an imaging system and discusses signal processing techniques. Doppler and color flow imaging are deferred until the next chapter. An amazing variety of transducer types have been invented and adapted to specific clinical uses; therefore, the major clinical uses of ultrasound imaging systems need to be considered also.

In Figure 10.1, the external parts of an ultrasound imaging system are shown. The image display is mounted on a chassis with wheels for portability. On the right side,
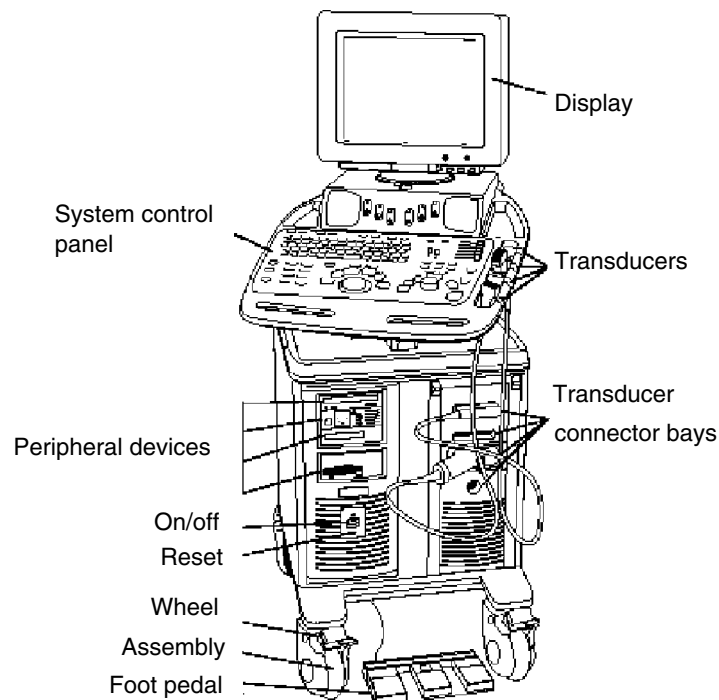
Figure 10.1   External parts of an ultrasound imaging system (courtesy of Philips Medical Systems).

several transducer arrays are stored, awaiting use, and they are attached to the system through several transducer connector bays in the front. Below the display is a keyboard and a number of knobs and switches for controlling the system. Peripheral devices, such as recording media and extra connectors, can be seen. The all-important on/off switch, which is sometimes difficult to find, is also identified.

10.2   TRENDS IN IMAGING SYSTEMS

Ultrasound imaging systems fall into the following commonly used categories: portable, low-end, mid-range, and high-end. The high-end systems are those with the latest and largest number of state-of-the-art features, and they generally produce the best images. Each manufacturer has unique features, called market differentiators, which distinguish their system from others manufactured by the same company, as well from those made by other companies. Over time, some features, because of the competitive nature of the industry, may migrate in altered form to imaging systems of rival manufacturers. Needless to say, because high-end systems have the most features and options, they are the most expensive. A mid-range system does not have some of the high-end features but has a full complement of options necessary to produce very good images in a variety of clinical applications. Low-end systems are usually limited in their functionality and are often designed to cover specific clinical applications. There are exceptions to these general categories.

The ultrasound imaging industry is undergoing dynamic change. One trend is that the new high-end features tend to migrate downward to mid-range systems and eventually to low-end systems over time. This migration is in part caused by the need to replace existing features with new ones to grow the market. Another major force is the parallel development in allied fields such as computation and electronics of enabling technologies (the invisible wind of change discussed in Chapter 1). These developments have already had a profound effect on what is possible with ultrasound as exemplified by the fully functional, portable imaging systems now available.

Portable imaging systems, which are a relatively new development, may provide a more restricted range of options (e.g., fewer transducers) or be fully functional with several transducer options in an extremely small package at a very low cost. Four portable systems were shown in Figure 1.13.

The Minivisor, the first fully portable, self-contained imaging system (mentioned in Chapter 1), is included for historical reference. The Sonosite system was the first modern portable of comparable size (about 6 lbs) and achieved its portability through custom designed ASICS. OptiGo, a portable also based on specialized chips, was designed for cardiac applications. Both of these systems offer color flow imaging and automated features to aid users. The Terason 2000 system achieves its small size and flexibility by leveraging laptop technology and its unique proprietary low power charge domain processor chip. The fully functional 128-channel system consists of a laptop, a 10-oz processor box, and the transducer. These systems were featured in an issue of the *Thoraxcentre Journal* (2001).

10.3 MAJOR CONTROLS

Because there are many controls for a typical ultrasound imaging system and their organization and names vary considerably from manufacturer to manufacturer, the following description is a short list of the major controls according to function. Note that even though the number of actual controls on an imaging system may seem bewildering at first, most systems start in a default set of control settings or ''presets'' that are optimized for a particular clinical application or transducer, so that with clinical training and moderate effort, such as the adjustment of time gain compensation (TGC) controls, a reasonably good image can be obtained quickly.

A close-up of the system control panel of the same imaging system from Figure 10.1 is illustrated in Figure 10.2. On the right side, the TGC slide controls, transmit focus controls, and scan depth controls are evident.

The main controls identified in the system control panel (depicted in Figure 10.2) are the following:

Probe or transducer selection: Typically two to four transducers can be plugged into connectors in the imaging system, so this switch allows the user to activate one of the arrays at a time.

Mode selection: This provides the means for selecting a mode of operation, such as 2B-mode, color flow, M-mode, or Doppler, individually or in combination (duplex or triplex operation).

Depth of scan control: This adjusts the field of view (scan depth in centimeters).

Focus or transmit focal length selection: This allows the location of the transmit focal length to be moved into a region of interest. The depth location of the focal plane is usually indicated by a > symbol. (Multiple transmit foci can be selected in a
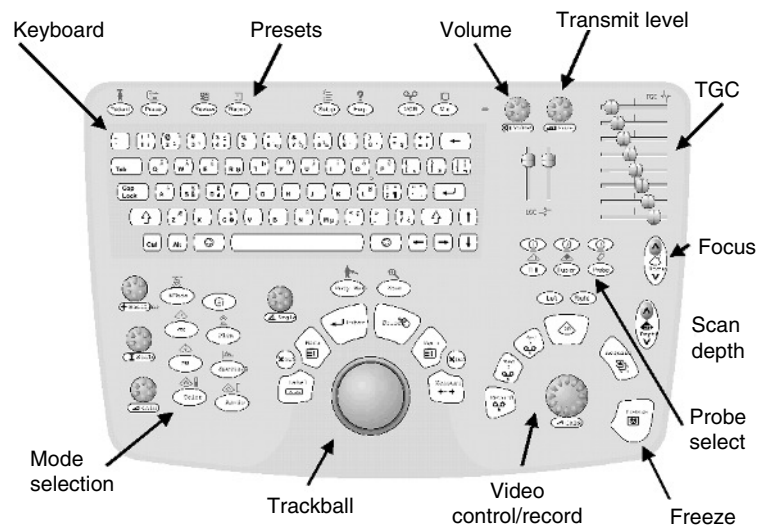
Figure 10.2   Keyboard and display of an ultrasound imaging system (courtesy of Philips Medical Systems).

splice or multiple transmit mode at the sacrifice of frame rate). In pulsed wave Doppler mode, the location of the focal length is often controlled by the center of the Doppler gate position.

Time gain compensation (TGC) controls (also depth gain compensation, time gain control, sensitivity-time control, etc.): These controls offset the loss in signal caused by tissue absorption and diffraction variations; they are usually in the form of slides for controlling amplifier gain individually in each contiguous axial time range. The image depth dimension is divided into a number of zones or stripes, each of which is controlled by a TGC control (discussed in Section 4.6). On some systems, these gains are adjusted automatically based on signal levels in different regions of the image. Some systems also provide the capability to adjust gains in the lateral direction (lateral gain compensation or additional control in the horizontal dimension). Other systems may have an automatic means of setting these controls based on parameters sensed in the signals in the image, sometimes called "automatic TGC."

Transmit level control: This adjusts drive amplitude from transmitters (it is done automatically on some systems). In addition to this control, a number of other factors alter acoustic output (discussed in more detail in Chapters 13 and 15). Feedback on acoustic output level is provided by thermal and mechanical indices on the display (also discussed in more detail in Chapters 13 and 15). A freeze control stops transmission of acoustic output.

Display controls: Primarily, these controls allow optimization of the presentation of information on the display and include a logarithmic compression control, selection of preprocessing and postprocessing curves, and color maps, as well as the ability to adjust the size of the images from individual modes selected for multimode operation. Provision is usually available for recording video images, playing them back, and comparing and sending them in various formats.

10.4 BLOCK DIAGRAM

The hidden interior of a digital imaging system is represented functionally by a generic simplified block diagram (shown by Figure 10.3). For now, the general operation of an imaging system is discussed (more details will be presented later).

A description of this block diagram follows:

User interface: Most of the blocks are hidden from the user, who mainly sees the keyboard and display, which are part of a group of controls called the "user interface." This is the part of the system by which the user can configure the system to work in a desired mode of operation. System displays showing software configurable menus and controls (soft-keys) in combination with knobs or slider controls and switches, as well as the main image display monitor, provide visual feedback that the selected mode is operating. The user interface provides the means of getting information in and out of the system through connectors to the system. Main connections include a computer hookup to a local area network (LAN) to Digital Imaging and Communication in Medicine (DICOM) communication and networking, and to peripherals such as
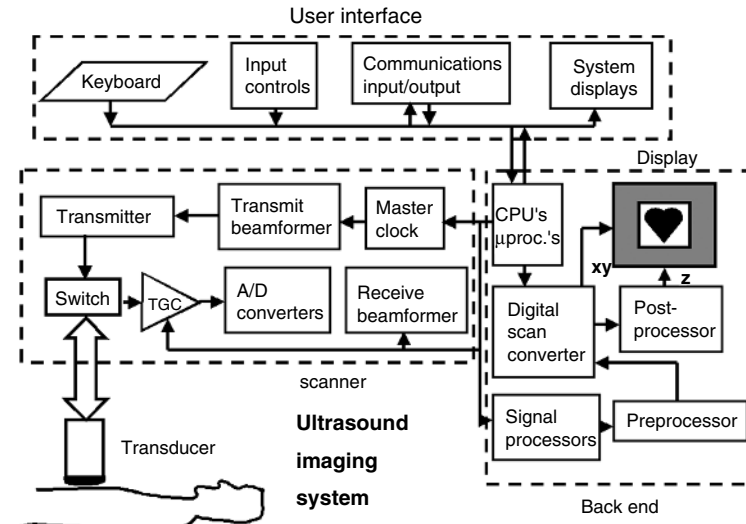
Figure 10.3   Block diagram of a generic digital ultrasound imaging system.

printers. Various recording devices, such as VCRs, and memory storage devices, such as read/write CD-ROMs and DAT drives, can be attached.

Controller (computers): A typical system will have one or more microprocessors or a PC that directs the operation of the entire system. The controller senses the settings of the controls and input devices, such as the keyboard, and executes the commands to control the hardware to function in the desired mode. It orchestrates the necessary setup of the transmit and receive beamformers as well as the signal processing, display, and output functions. Another important duty of the computer is to regulate and estimate the level of acoustic output in real time.

Front end: This grouping within the scanner is the gateway of signals going in and out of the selected transducer. Under microprocessor transmit control, excitation pulses are sent to the transducer from the transmitter circuitry. Pulse-echo signals from the body are received by array elements and go through individual user-adjustable TGC amplifiers to offset the weakening of echoes by body attenuation and diffraction with distance. These signals then pass on to the receive beamformer.

Scanner (beamforming and signal processing): These parts of the signal chain provide the important function of organizing the many signals of the elements into coherent timelines of echoes for creating each line in the image. The transmit beamformer sends pulses to the elements. Echo signals pass through an analog-to-digital (A/D) converter for digital beamforming. In addition, the scanner carries out signal processing, including filtering, creation of quadrature signals, and different modes such as Doppler and color flow.

Back end: This grouping of functions is associated with image formation, display, and image metrics. The input to this group of functions is a set of pulse-echo envelope lines formed from each beamformed radiofrequency (RF) data line. Image formation is achieved by organizing the lines and putting them through a digital scan converter

that transforms them into a raster scan format for display on a video or PC monitor. Along the way, appropriate preprocessing and postprocessing, log compression, and color or gray-scale mapping are completed. Image overlays containing alpha-numeric characters and other information are added in image planes. Also available in the back end are various metric programs, such as measuring the length of a fetal femur, calculating areas, or performing videodensitometry. Controls are also available for changing the format of the information displayed.

10.5 MAJOR MODES

The following are major modes on a typical imaging system:

Angio (mode): This is the same as the power Doppler mode (see Figure 11.23).

B-mode: This is a brightness-modulated image in which depth is along the z axis and azimuth is along the x axis. It is also known as "B-scan" or "2D mode." The position of the echo is determined by its acoustic transit time and beam direction in the plane. Alternatively, an imaging plane contains the propagation or depth axis (see Figure 9.1).

Color flow imaging (mode): A spatial map is overlaid on a B-mode gray-scale image that depicts an estimate of blood flow mean velocity, indicating the direction of flow encoded in colors (often blue away from the transducer and red toward it), the amplitude of mean velocity by brightness, and turbulence by a third color (often green). It is also known as a "color flow Doppler." Visualization is usually two-dimensional (2D) but can also be three-dimensional (3D) or four-dimensional (4D) (see Figure 10.6a).

Color M-mode: This mode of operation has color flow depiction at the same vector location where depth is the y deflection (fast time), and the x deflection is the same color flow line shown as a function of slow time. This mode displays the time history of a single color flow line at the same spatial position over time (see Figure 11.24).

Continuous wave (CW) Doppler: This Doppler mode is sensitive to the Doppler shift of blood flow all along a line (see Figure 11.13).

M-mode: This mode of operation is brightness modulated, where depth is the y deflection (fast time), and the x deflection is the same imaging line shown as a function of slow time. This mode displays the time history of a single line at the same spatial position over time (see Figure 10.4).

Doppler mode: This is the presentation of the Doppler spectrum (continuous wave or pulsed wave).

Color Doppler (mode): A 2D Doppler image of blood flow is color-coded to show the direction of flow to and away from the transducer (see Figure 10.6a).

Power Doppler (mode): This color-coded image of blood flow is based on intensity rather than on direction of flow, with a paler color representing higher intensity. It is also known as "angio" (see Figure 11.23).

Pulsed wave Doppler: This Doppler mode uses pulses to measure flow in a region of interest (see Figures 11.15 and 11.21).

Duplex: Presentation of two modes simultaneously: usually 2D and pulsed (wave) Doppler (see Figure 10.5).
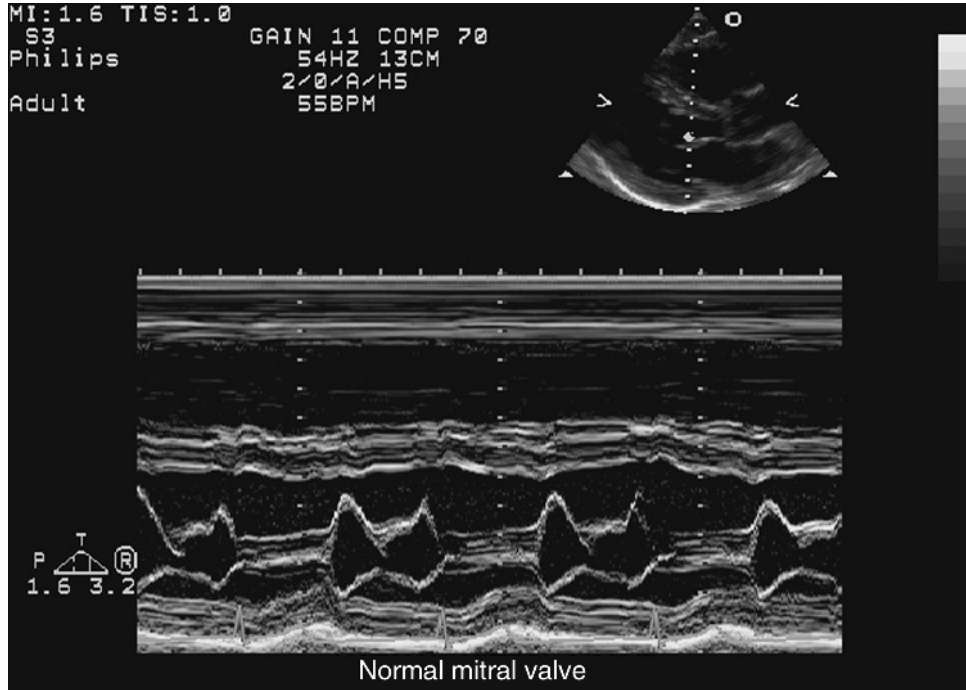
Figure 10.4   Duplex M-mode image. The insert (above right of the sector image) shows the orientation of the M-mode (courtesy of Philips Medical Systems).
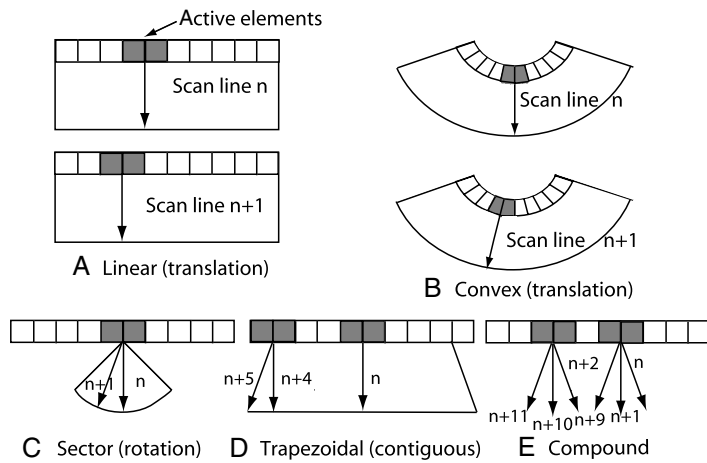
Figure 10.5   Time-sequenced image formats. (A) Basic linear (translation). (B) Convex curved linear (translation). (C) Basic sector (rotation). (D) Trapezoidal (contiguous: rotation, translation, and rotation). (E) Compound (translation and rotation at each active aperture position).
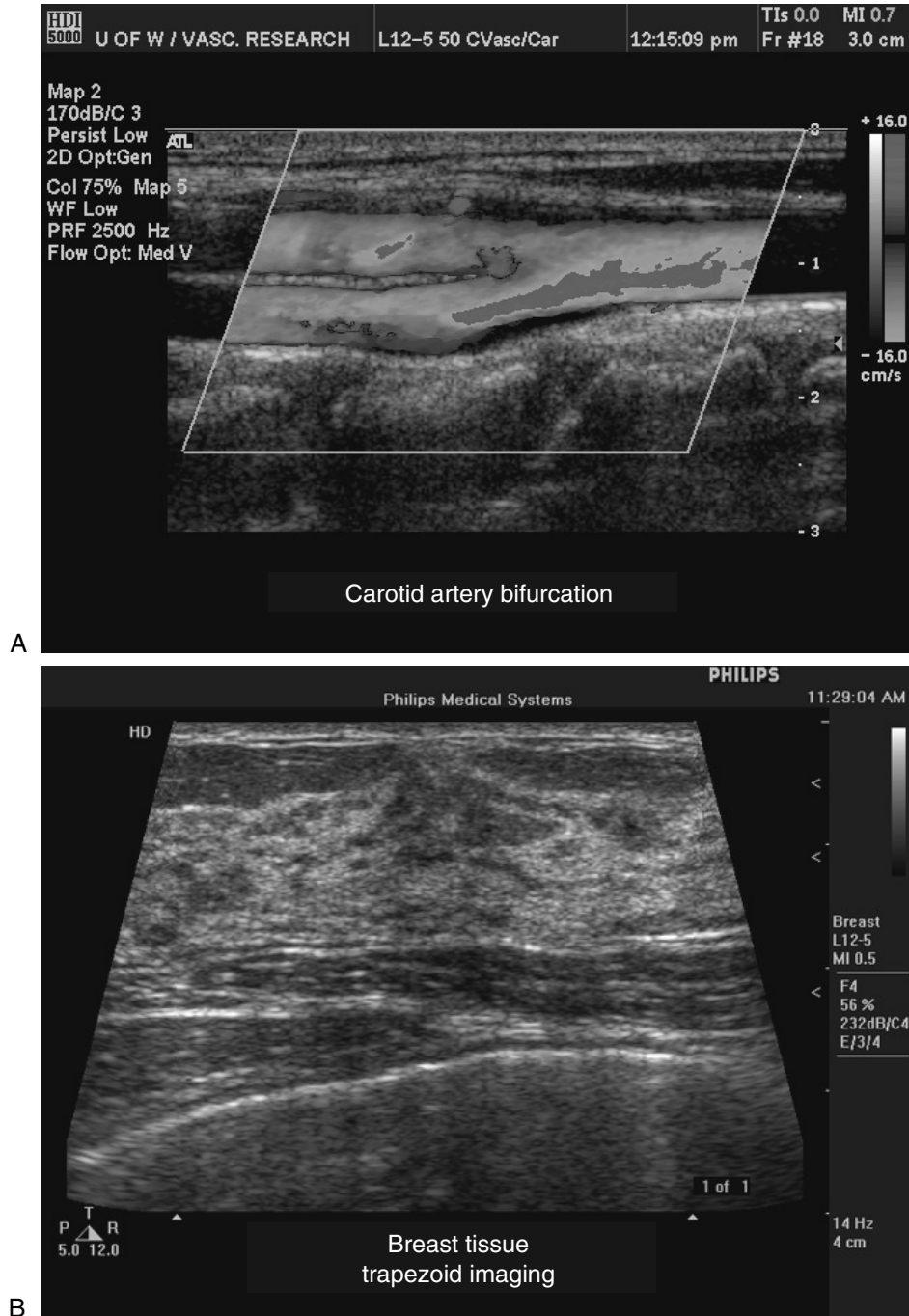
Figure 10.6 (A) Parallelogram-style color flow image from a linear array with steering. (B) Trapezoidal form at of a linear array with sector steering on either side of a straight rectangular imaging segment. Described as a contiguous imaging format in Chapter 1 (courtesy of Philips Medical Systems) (see also color insert).

Triplex: Presentation of three modes simultaneously: usually 2D, color flow, and pulsed Doppler (see Figures 11.13 and 11.15)

2D: (B-mode) imaging in a plane, with the brightness modulated

3D: This is a image representation of a volume or 3D object, such as the heart or fetus. Surface rendering can be used to visualize surfaces. Another image presentation is volume rendering, in which surfaces can be semitransparent or 2D slice planes through the object. Alternatively, there is simultaneous viewing of different 2D slice planes (side by side).

4D: A 3D image moving in time

Zoom: Video zoom is a magnification of a region of interest in the video image. Alternatively, acoustic zoom is a magnification of the region of interest in which acoustic and/or imaging parameters are modified to enhance the image, such as placing the transmit focus in the region of interest and/or increasing the number of image lines in the region.

10.6 CLINICAL APPLICATIONS

Diagnostic ultrasound has found wide application for different parts of the human body, as well as in veterinary medicine. The major categories of ultrasound imaging are listed below.

Major Imaging Categories:

Breast: Imaging of female (usually) breasts

Cardiac: Imaging of the heart

Gynecologic: Imaging of the female reproductive organs

Radiology: Imaging of the internal organs of the abdomen

Obstetrics (sometimes combined with Gynecologic as in OB/GYN): Imaging of fetuses *in vivo*

Pediatrics: Imaging of children

Vascular: Imaging of the (usually peripheral as in peripheral vascular) arteries and veins of the vascular system (called "cardiovascular" when combined with heart imaging)

Specialized applications have been honored by their own terminology. Many of these terms were derived from the location of the acoustic window where the transducer is placed, as well as the application. "Window" refers to an access region or opening through which ultrasound can be transmitted easily into the body. Note that transducers most often couple energy in and out of the body through the use of an externally applied couplant, which is usually a water-based gel or fluid placed between the transducer and the body surface. Transducers, in addition to being designed ergonomically to fit comfortably in the hand for long periods of use, are designed with the necessary form factors to provide access to or through the windows described later.

Major Imaging Applications:

(Note that "intra" (from Latin) means into or inside, "trans" means through or across, and "endo" means within.)

Endovaginal: Imaging the female pelvis using the vagina as an acoustic window

Intracardiac: Imaging from within the heart

Intraoperative: Imaging during a surgical procedure

Intravascular: Imaging of the interior of arteries and veins from transducers inserted in them

Laproscopic: Imaging carried out to guide and evaluate laparoscopic surgery made through small incisions

Musculoskeletal: Imaging of muscles, tendons, and ligaments

Small parts: High-resolution imaging applied to superficial tissues, musculature, and vessels near the skin surface

Transcranial: Imaging through the skull (usually through windows such as the temple or eye) of the brain and its associated vasculature

Transesophageal: Imaging of internal organs (especially the heart) from specially designed probes made to go inside the esophagus

Transorbital: Imaging of the eye or through the eye as an acoustic window

Transrectal: Imaging of the pelvis using the rectum as an acoustic window

Transthoracic: External imaging from the surface of the chest

10.7   TRANSDUCERS AND IMAGE FORMATS

10.7.1   Image Formats and Transducer Types

Why do images come in different shapes? The answer depends on the selected transducer, without which there would be no ultrasound imaging system. Our discussion emphasizes types of arrays (the most prevalent form of transducers in ultrasound imaging). The focus will be on widely used physical forms of arrays adapted for different clinical applications and their resulting image formats.

Early ultrasound imaging systems employed single-element transducers, which were mechanically scanned in an angular or linear direction or both (as described in Chapter 1). Most of these transducers moved in a nearly acoustically transparent cap filled with a coupling fluid. The first practical arrays were annular arrays that consisted of a circular disk cut into concentric rings, each of which could be given a delayed excitation appropriate for electronic focusing along the beam axis. These arrays also had to be rotated or scanned in a cap, and they provided variable focusing and aperture control for far better imaging than is available with fixed-focus, single-element transducers. A detailed description of the design and performance of a real-time, digital 12-element annular array ultrasound imaging system is available in Foster *et al*. (1989a, 1989b).

Another early array was the linear array (discussed in Chapter 1). The linear array may have up to 300–400 elements, but at any specific time, only a few (forming an active element group) are functioning at a time. The active contiguous elements form the active aperture. At one end of the array, an active element group turns on, as selected by a multiplexer (also called a "mux") that is receiving commands from the beamformer controller. Refer to Figure 10.5a, where the active elements are shaded to generate line number n. After the first pulse echoes are received for the first image

vector line (centered in the middle of this group), an element nearest the end of the array is switched off and the element next to the other end of the group is added as a new element. In this way, the next sequential line (numbered $n+1$) is formed, and this "tractor-treading" process continues as the active group slides along the length of the array, picking up and dropping an element at each line position. Switches are necessary if the number of elements in the array exceeds the number of receive channels available. The overall image format is rectangular in shape.

The main difference between a linear and a phased array is steering. The phased array has an active aperture that is always centered in the middle of the array, but the aperture may vary in the number of elements excited at any given time (discussed shortly). As shown in Figure 10.5c, the different lines are formed sequentially by steering until a sector (an angular section of a circle), usually about 90° in width, is completed. The phased array has a small "footprint" or contact surface area with the body. A common application for this type of an array is cardiac imaging, which requires that the transducer fit in the intercostal spaces between the ribs (typically 10–14 mm). The advantage of this array is that despite its small physical size, it can image a large region within the body.

Because it was easier to produce a fixed focal delay without steering for each line, linear arrays were the first to appear commercially (recall Chapter 1). In this tradition, convex linear arrays combined the advantage of a larger angular image extent with ease of linear array focusing without the need for electronic steering. Convex arrays may be regarded as linear arrays on a curved surface. As depicted in Figure 10.5b, a convex array has a similar line sequencing to a linear array except that its physical curvature directs the image line into a different angular direction. Because of the lack of steering, linear and convex arrays have a relaxed requirement for periodicity 1–3 wavelengths rather than the ½ wavelength usually used for phased arrays.

Recent exceptions to this approach are linear arrays with finer periodicity so that they can have limited steering capability either for Doppler or color flow imaging. In this case, once the extent of steering is decided, periodicity can be determined from grating lobe calculations (see Chapter 7). Two common applications are parallelogram (also known as a steered linear) and trapezoidal imaging, in which sector-steered image segments are added to the ends of a rectangular image in a contiguous fashion (shown in Figure 10.5d). Actual imaging examples are given by Figure 10.7.

Another use of more finely sampled linear arrays with steering capabilities is compound imaging. As shown in Figure 10.5e, compound imaging is a combination of limited steering by an active group and translation of the active group to the next position for the next set of lines or image vectors. More information and imaging examples of a real-time implementation of this method will be discussed in Section 10.11.4.

The number of active elements selected for transmission is usually governed by a constant F number (F#). The −6-dB full width half maximum (FWHM) beamwidth can be shown to be approximately $FWHM = 0.4\lambda F/L = 0.4\lambda F\#$ from Eq. (6.9c). To achieve a constant lateral resolution for each deeper focal length (F), the aperture (L) is increased to maintain a constant F# until the full aperture available is reached. In a typical image, one transmit focal length is selected along with dynamic focusing on
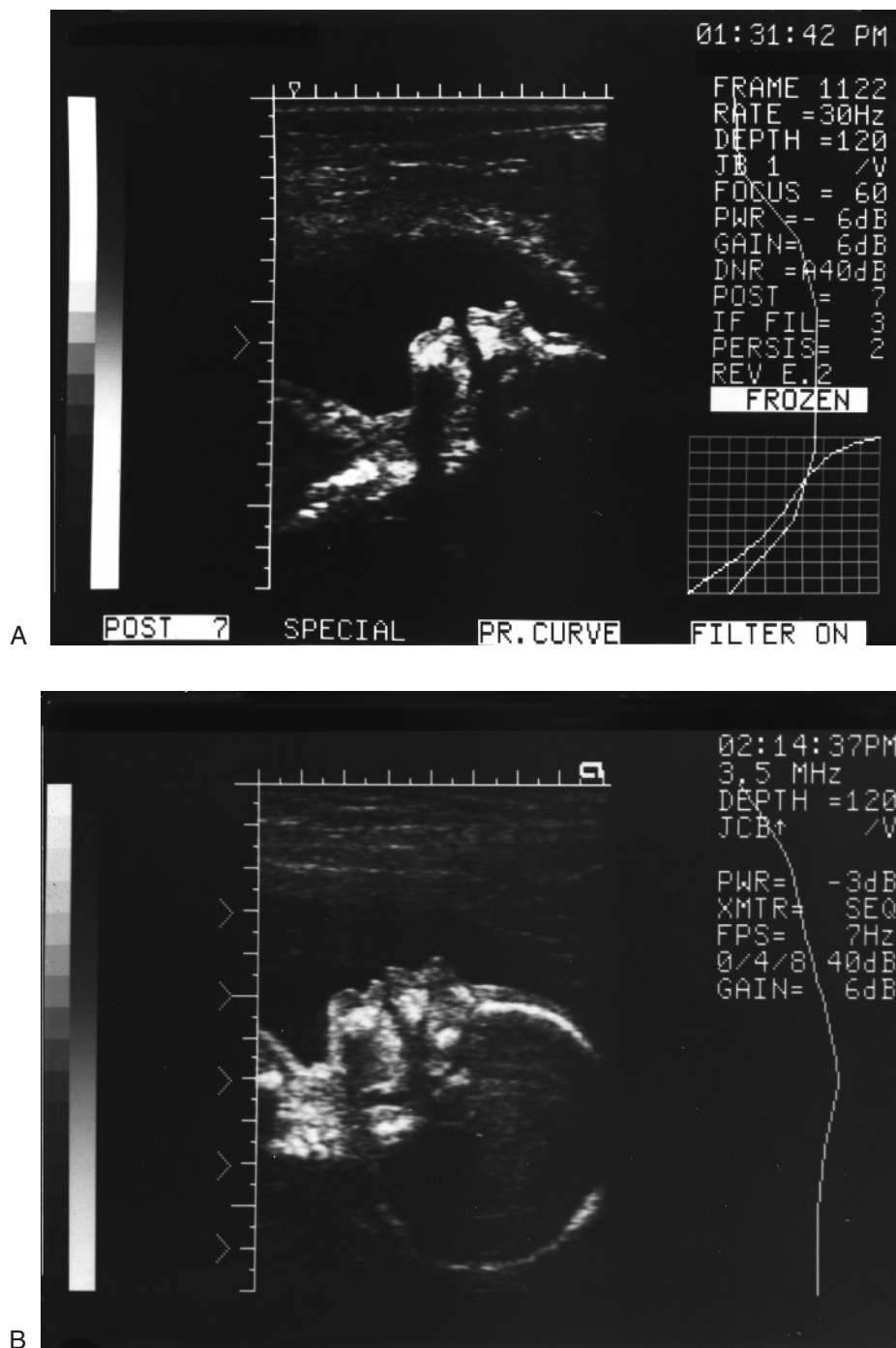
Figure 10.7 Transmit focusing of fetal head with (A) a single focus zone and (B) multiple spliced focal zones (courtesy of Siemens Medical Solutions, Inc. Ultrasound Group).

Figure 10.8   SieScape or panoramic image made by a transducer swept along a body surface (courtesy of Siemens Medical Solutions, Inc. Ultrasound Group).

receive. At the expense of frame rate, it is possible to improve resolution by transmitting at several different transmit focal lengths in succession and then splicing together the best parts. The strips or time ranges contain the best lateral resolution (like a layer cake) to make a composite image of superb resolution (Maslak, 1985). See Figure 10.7 for an example. For this method, a constant F# provides a similar resolution in each of the strips as focal depth is increased.

To overcome the small field of view limitation in typical ultrasound images, a method of stitching together a panoramic view (such as that shown in Figure 10.8) was invented. Even though the transducer is scanned freehand across the skin surface to be imaged, advanced image processing is used to combine the contiguously scanned images in real time (Tirulmalai *et al.*, 2000). Other modes can also be shown in this type of presentation.

10.7.2 Transducer Implementations

Driven by many clinical needs, transducers appear in a wide variety of forms and sizes (as indicated by Figure 10.9). From left to right in this figure, there is a transesophageal probe mounted on the end of a gastroscope, a convex array, a linear array,

Figure 10.9 Transducer family portrait. From left to right, transesophageal array with positioning assembly, convex (curved) linear array, linear array, stand alone CW Doppler probe, phased array, transthoracic motorized rotatable phased array, and high-frequency intraoperative linear array (courtesy of Philips Medical Systems).

a "stand-alone" CW Doppler two-element transducer, a phased array, a motorized transthoracic array with an internal motor drive for 3D acquisition, and an intraoperative probe. The transesophageal probe (shown at the tip in the top center of the figure) is mounted in a gastroscope assembly (at extreme left of figure) to provide flexible positioning control of the transducer attitude within the throat. Transesophageal arrays couple through the natural fluids in the esophagus and provide cleaner windows to the interior of the body (especially the heart) than transducers applied externally through body walls. The endovaginal and transrectal probes (not shown) are designed to be inserted. The intraoperative and specialty arrays provide better access for surgical and near-surface views in regions sometimes difficult to access. These probes can provide images before, during, or after surgical procedures.

The more conventional linear, curved linear, and phased arrays have typical azimuth apertures that vary in length from 25 to 60 mm and elevation apertures that are 2–16 mm, depending on center frequency and clinical application. Recall that the aperture size in wavelengths is a determining factor. The number of elements in a 1D array vary from 32 to 400. Typical center frequencies range from 1 MHz (for

harmonic imaging) to 15 MHz (for high-resolution imaging of superficial structures). As discussed in Chapter 6, there has been a trend toward wider fractional bandwidths, which now range from 30–100%.

At first, array systems functioned at only one frequency because of the narrow fractional bandwidth available. As transducer design improved, wider bandwidth allowed for operation at a higher imaging frequency simultaneously with a lower-frequency narrowband Doppler or color flow mode (as indicated in Figure 10.10b). This dual frequency operation was made possible by two different transmit frequencies combined with appropriate receive filtering, all operating within the transducer bandwidth. The next generation of transducers made possible imaging at more than one frequency, as well as operation of the Doppler-like modes (see Figure 10.10c). At the present time (with new materials), this direction is continuing so that a single transducer array can function at multiple center frequencies (as shown in Figure 10.10d). This type of bandwidth means that one transducer can replace two or three others, permit harmonic imaging with good sensitivity, and provide higher image quality (to be described in Section 10.11.3). Broad bandwidths are also essential for harmonic imaging (to be described in Chapter 12).
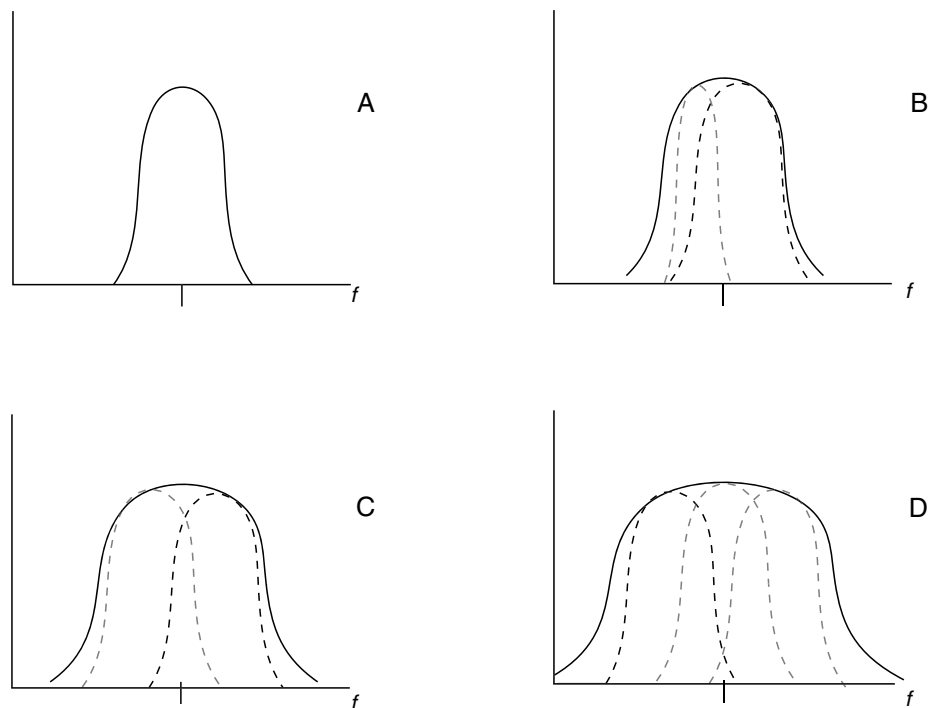
Figure 10.10 Stages of transducer bandwidth development. (A) Narrowband. (B) Dual mode. (C) Multiple mode. (D) Very wide band.

10.7.3   **Multidimensional Arrays**

As discussed in Chapter 7, most arrays are 1D with propagation along the z axis and electronic scanning along the x axis to form the imaging plane. Focusing in the elevation or yz plane is accomplished through a fixed focal length lens. A hybrid approach (a 1.5D array) achieves electronic focusing in the elevation plane by forming a coarsely sampled array in the y dimension at the expense of more elements. This number is a good compromise, however, compared to a complete 2D array, which usually requires about an n^2 channel count compared to n channels for 1D arrays. A way of reducing the number of electronic channels needed is to decrease the active number of elements to form a sparse array. All of these considerations were compared in Chapter 7. The main advantages of electronic focusing in the elevation are not only flexibility, but also improved resolution from coincident focusing in both planes and dynamic receive focusing in both planes simultaneously. The description of a real-time, fully populated 2D array with a nonstandard architecture is postponed until Section 10.11.6.

10.8   **FRONT END**

The front end is the mouth of the imaging system; it can talk and swallow. It has a number of channels, each of which has a transmitter and a switch (including a diode bridge) that allows the passage of high voltage transmit pulses to the transducer elements but blocks these pulses from reaching sensitive receivers (refer to the block diagram of Figure 10.3). Echoes return to each receiver, which consists of amplifiers in series, including one that has a variable gain for TGC under user control. The output of each channel is passed on to the receive beamformer.

10.8.1   **Transmitters**

The heartbeat of the system is a series of synchronized and precisely timed primitive excitation pulses (illustrated by Figure 10.11). The major factor in this heartbeat is the scan depth selected (s_d). The length of a line or vector, since each line has a vector direction, is simply the round-trip travel time ($2s_d/c_0$). As soon as one line has completed its necessary round-trip time, another line is launched in the next incremental direction required. For a simple linear array, the next line is parallel to the last one, whereas in a sector format, the next line is incremented through steering by a small angle.

The timing pulses associated with these events are the start of frame pulse, followed by the start of transmit. This last pulse actually launches a group of transmit pulses in parallel with the required delays to form a focused and steered beam from each active array element. The exact timing of these transmit pulses was described in Chapter 7. This process is repeated for each vector until the required number of lines (N) has been completed, after which a new start-of-frame timing pulse is issued by the system transmitter clock.
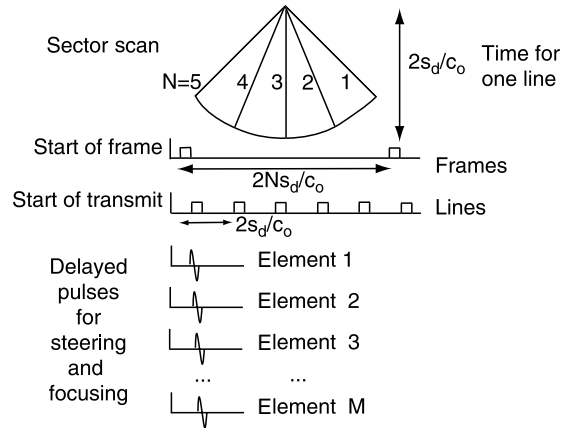
Figure 10.11 Pulse generation sequencing in an imaging system.

The rhythm of the system heartbeat can be interpreted as a repetitive timing sequence with a duty cycle. For the example shown in Figure 10.11, assume a scan depth of $s_d = 150$ mm, as well as 5 lines per frame and 6 active elements. The round-trip time for one line is $2s_d/c = 200$ μs; this will be the start of the transmit pulse interval between each line. The time for a full frame is N lines/frame or, in this case, 5×200 μs/frame $= 1000$ μs/frame or 1000 frames/sec. The number of lines is only 5 for this example. A more realistic number of lines is 100, in which case the time for a full frame would be 20 ms or a frame rate of 50 frames/sec.

Finally, depicted in the bottom of Figure 10.11 is a sequence of delayed pulses (one for each active element of the array) to steer and focus the beam for that line. Note that these pulses are launched in parallel with each start of transmit. These transmit pulses have a unique length or shape for the mode and frequency chosen. For example, instead of one primitive transmit pulse such as a single cycle of a sine wave for 2D imaging, a number (m) of primitive pulses in succession can be sent to form an elongated pulse for Doppler mode. The duty cycle is taken to be the ratio of the length of the basic transmit sequence per line divided by the round-trip time. In practice, a vector line may be repeated by another one in the same direction or by one in a different mode in a predetermined multimode sequence necessary to build a duplex or a triplex image (Szabo *et al.*, 1988).

10.8.2 Receivers

In order to estimate the dynamic range needed for a front end, typical echo levels in cardiac imaging will be examined. Numbered amplified backscattered echoes from the heart are illustrated by Figure 10.12b for the beam path shown through a cross section of the heart in Figure 10.12a (Shoup and Hart, 1988). With reference to the indexing of the echoes, the first waveform corresponds to feed-through during the

A

B

Echo no.   1   2   3   4   5   6   7
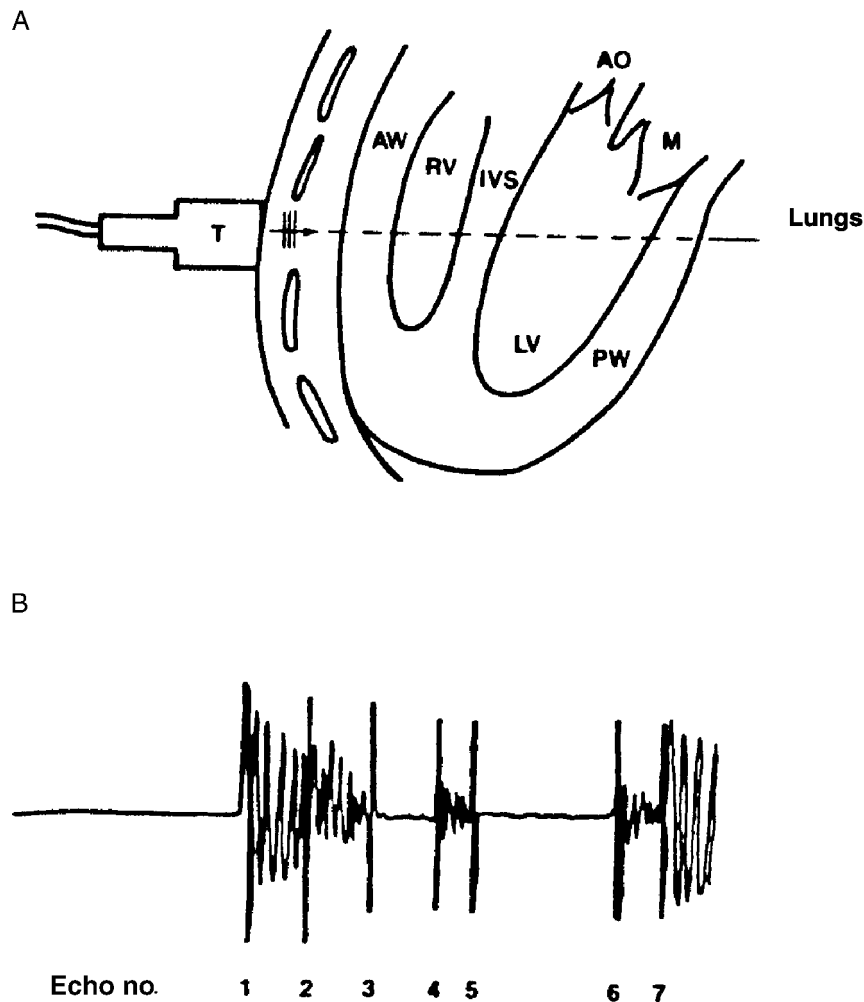
Figure 10.12   (A) Echo path through the heart. AW = anterior wall, RV = right ventricle, IVS = intraventricular septum, LV = left ventricle, AO = aortic valve, M = mitral valve, PW = posterior wall. (B) Amplified echoes corresponding to path in (A) (from Shoup and Hart, 1988, *IEEE*).

excitation pulse. Echo 2 is caused by the reflection factor (RF) between the fat in the chest wall and muscle of the anterior wall; this kind of signal is on the average about −55 dB below that obtained from a perfect (100%) reflector. Echo 3 is the echo from the reflection between blood and the tissue in the wall; it has a similar absolute level. Between echoes 3 and 4 is the backscatter from blood, which is at the absolute level of −70 dB compared to a 100% reflector and falls below the scale shown. The large echo number 7 is from the posterior wall lung interface; it is a nearly perfect reflector (close to 0 dB absolute level). In order to detect blood and the lung without saturating, the

receivers require a dynamic range of at least 70 dB for cardiac imaging. TGC amplification (mentioned in Chapter 4) was applied to the echoes in Figure 10.12b. The absolute values of the echoes were determined independently from RF data and a reference reflector. There is an individual front-end amplifier for each channel (usually 64 or 128 total) in the system. Each amplifier typically covers a range of 55–60 dB. For digital conversion, sampling rates of 3–5 times the highest center frequency are needed to reduce beamforming quantization errors (Wells, 1993). A means of time shifting for the dynamic receive beamformer at higher rates, closer to 10 times the center frequency, would be preferable to achieve low beam sidelobes (Foster *et al.*, 1989). Modern imaging systems can have dynamic ranges in excess of 100 dB, and some have the sensitivity to image blood directly in B-mode at high frequencies (see Chapter 11) and to detect weak harmonic signals (see Chapters 14 and 15).

10.9   SCANNER

10.9.1   Beamformers

In Chapter 7, the operation of transmit and receive beamformers was discussed. The practical implementation of these beamformers involves trade-offs in time and amplitude quantization. In addition, more complicated operations have been implemented. In order to speed up frame rate, basic parallel beamforming is a method of sending out a wide transmit beam and receiving several receive beams (as explained in Section 7.4.3). The discussion of real-time compound imaging (Entrekin *et al.*, 2000), which involves the ability of the beamformer to send out beams along multiple vector directions from the same spatial location in a linear array, is deferred until Section 10.11.4.

10.9.2   Signal Processors

10.9.2.1   Bandpass filters

This signal processing part of the system takes the raw beamformed pulse-echo data and selectively pulls out and emphasizes the desired signals, combines them as needed, and provides real and quadrature signals for detection and modal processing. This section covers only processing related to B-mode imaging. Chapter 11 covers color flow imaging and Doppler processing. Digital filters operate on the data from the A/D converters (shown in the block diagram, Figure 10.3). Bandpass filtering is used to isolate the selected frequency range for the desired mode within the transducer passband (recall Figure 10.10). The data may also be sent to several bandpass filters to be recombined later in order to reduce speckle (see Section 10.11.3). Another important function of bandpass filtering is to obtain harmonic or subharmonic signals for harmonic imaging (to be covered in more detail in Chapter 12). In Chapter 4, absorption was shown to reduce the effective center of the signal spectrum with depth. The center frequency and shape of bandpass filters can be made to vary with depth to better track and amplify the desired signal (see Section 10.11.2).

10.9.2.2 Matched filters

Another important related signal processing function is matched filtering. In the context of ultrasound imaging, this type of filter has come to mean the creation of unique transmit sequences, each of which can be recognized by a matched filter. One of the key advantages of this approach is that the transmit sequence can be expanded in time at a lower amplitude and transmitted at a lower peak pressure amplitude level, with benefits for reducing bioeffects (see Chapter 15) and contrast agent effects (see Chapter 14). Other major advantages include the ability to preserve axial resolution with depth, and increased sensitivity and tissue penetration depth.

Matched filtering actually begins with the transmit pulse sequence. In this case, the transmit waveform is altered into a special shape or sequence, $s(t)$. This transmission encoding can be accomplished by sending a unique sequence of primitive pulses of different amplitudes, polarities, and/or interpulse intervals. In the case of binary sequences, a "bit" is a primitive pulse unit that may consist of, for example, half an RF cycle or several RF cycles.

Two classic types of transmit waveforms, $x(t)$, a coded binary sequence and a chirped pulse, have been borrowed from radar and applied to medical ultrasound (Lee and Ferguson, 1982; Lewis, 1987; Cole, 1991; O'Donnell, 1992; Chiao and Hao, 2003). The appropriate matched filter in these cases is $x^*(-t)$. The purpose of a matched filter is to maximize signal-to-noise, defined as the ratio of the peak instantaneous output signal power to the root mean square (r.m.s.) output noise power (Kino, 1987). A simple explanation of how the output power can be maximized can be given through Fourier transforms. Consider a filter response,

$$y(t) = x(t) * h(t) \tag{10.1}$$

where $x(t)$ is the input, $y(t)$ is the output waveform, and $h(t)$ represents the filter. Let the matched filter be

$$h(t) = Ax^*(-t) \tag{10.2}$$

where A is a constant and $*$ represents the conjugate. For this filter, the output becomes

$$y(t) = Ax(t) * x^*(-t) = A \int_{-\infty}^{\infty} x(\tau)x^*(\tau - t)d\tau = A \int_{-\infty}^{\infty} x^*(\tau) x(\tau + t)d\tau \tag{10.3}$$

but from the Fourier transform, the output can be rewritten as

$$y(t) = A \int_{-\infty}^{\infty} X(f)X^*(f)e^{i2\pi ft}df = A \int_{-\infty}^{\infty} |X(f)|^2 e^{i2\pi ft}df \tag{10.4}$$

In other words, the matched filter choice of Eq. (10.2) leads to an autocorrelation function, Eq. (10.3), which automatically maximizes the power spectrum, Eq. (10.4) (Bracewell, 2000) and consequently, maximizes the ratio of the peak signal power to the r.m.s. noise power (Kino, 1987).

A simple example of a coded waveform is a three bit Barker code. This code can be represented graphically (shown in Figure 10.13), or it can be represented mathemati-
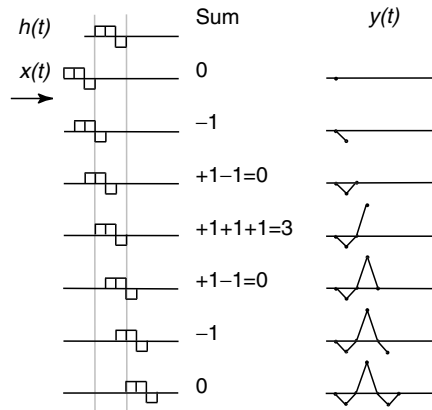
Figure 10.13 Output of a three-bit Barker code. (Top) Receive correlator sequence $h(t)$ versus time units. (Below) Input sequence $x(t)$ shown as incrementing one time unit or one bit at a time through the correlator with the corresponding summation and output waveform.

cally as the binary sequence $[+1+1-1]$. Binary codes have unique properties and solve the following mathematical puzzle: What sequence of ones and minus ones, when correlated with itself, will provide a gain in output (y) with low sidelobes?

In the top of Figure 10.13 is a plot of the correlation filter $h(t)$ against unit time increments. Recall that the convolution operation involves flipping the second waveform right to left in time and integrating (see Appendix A). Physically, correlation is the operation of convolution of $x(t) * x^*(-t)$. This integration consists of a double reversal in time (once for the convolution operation and once for the receive filter). The net result is a receive waveform that is back to its original orientation in time. The operation is simplified to sliding one waveform, $x(t)$, past the second, $x(t)$, left to right. Each row in this figure shows an input waveform sliding from left to right, one time unit interval at a time, until the waveform has passed through the correlator. Integration at each slot is easy: First, determine the amplitude values of $h(t)$ and $x(t)$ multiplied together, such as $-1 \times -1 = 1$, at each time interval overlap position; second, sum all the product contributions from each time interval in the overlap region to obtain the amplitude value for the time position in the row. In the last row, connect the dots at each time interval to get $y(t)$. The repeating triangular shapes within $y(t)$ can be recognized as the convolution, or correlation in this case, of two equal rectangles, $\Pi(t)$, that slide past each other to form triangle functions; these steps complete the description of $y(t)$ between the dots we calculated in Figure 10.13. Note the main features of $y(t)$: a peak equal to n bits (three) and two satellite time sidelobes of amplitude -1. From maximum amplitudes of plus or minus one, a gain of three has been achieved by encoding.

Fortunately, MATLAB makes these kinds of calculations trivial. We can obtain graphical results with three lines of code:

$$x = [0\ 1\ 1\ -1\ 0]';$$
$$y = x\,\text{corr}(x) \tag{10.5}$$
$$\text{plot}(y);$$

The first line forms the Barker sequence, allowing for zeros to get the full depiction of the output. The autocorrelation function is the cross-correlation function xcorr.m with one argument. The reader is encouraged to play with the program barkerplot.m to verify that as the number of bits, N, is increased, the peak increases in proportion and the ratio of peak amplitude level to maximum sidelobe level improves.

A family of codes with more impressive performance is the pseudo-random binary M-sequence code of ones and zeros that is shown in the lower right-hand corner of Figure 10.14 (Carr *et al.*, 1972) along with the output, $y(t)$. Here the sidelobe ratio is -15.84 dB. Note that for an acoustic transmitter, ones and zeros may translate into either a series of "ones" (regarded as positive primitive pulses, $+1$) and "zeros" (regarded as primitive pulses with a $180°$ phase reversal or negative-going pulses, -1).


Correlation-multiple tapped delay line-31 taps
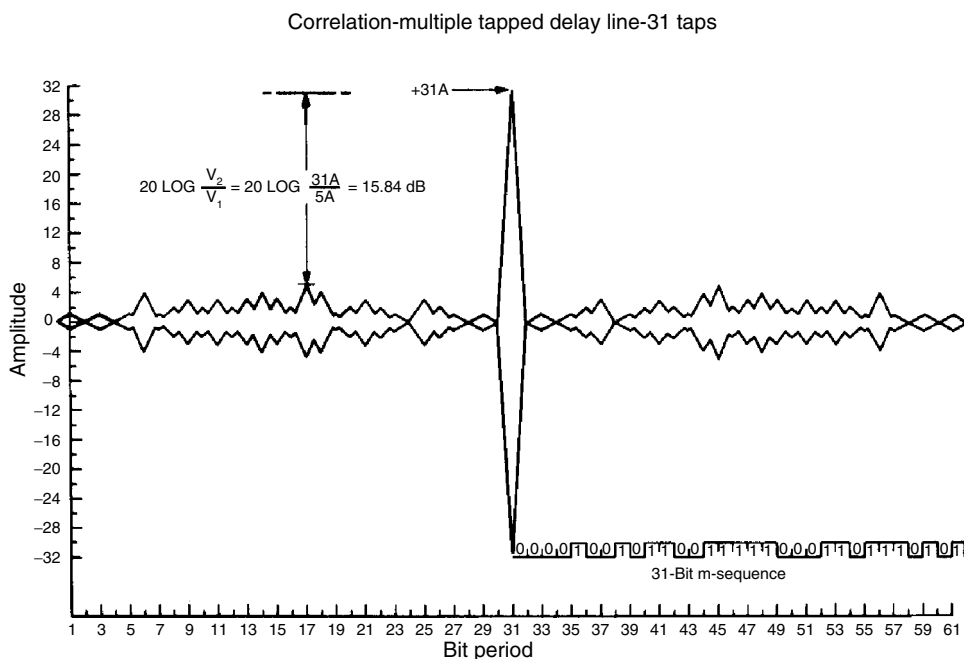
Figure 10.14 Theoretical plot of amplitude versus bit period for the correlation of a 31-bit maximal length (M) sequence. The peak-to-sidelobe ratio for this sequence is -15.84 dB (from Carr *et al.*, 1972, *IEEE*).

There are several families of codes, each with advantages and disadvantages. Each bit or primitive pulse alone will evoke a round-trip response from the transducer, which fixes the minimum resolution available. In the usual case without a coded sequence, a transmit pulse might consist of a half-period pulse or a full-period pulse (e.g., a single *sine* wave) corresponding to the desired frequency of excitation. Receive amplitude levels can be raised by increasing the applied transmit voltage. At some pressure level (described in Chapter 15), a fixed limit is reached for safety reasons so that the voltage can no longer be increased. One advantage of coded sequences is that a relatively low voltage A can be applied, and a gain of NA is realized on reception after the correlation process. Another advantage of coded sequences is that certain orthogonal codes, such as Golay codes, allow the simultaneous transmission of a number of beams in different vector directions, which are sorted out on decoded reception through matched correlators (Lee and Ferguson, 1982; Shen and Ebbini, 1996; Chiao *et al.*, 1997; Chiao and Hao, 2003) as is shown in Figure 10.15.

Another important class of coded matched filter functions are chirps (Lewis, 1987; Cole, 1991; Genis *et al.*, 1991). A methodology borrowed from radar, a transmit waveform, $x(t)$, consists of a linear swept frequency modulated (FM) pulse of duration T. The result of matched filtering is a high-amplitude short autocorrelation pulse. If a chirp extends over a bandwidth B, the correlation gain (G) through a matched filter $x^*(-t)$, a mirror image chirp, is $G = TB$ (Kino, 1987). Examples of a chirp and compressed pulses from flat targets are given in Figure 10.16. A third waveform depicts the transmitted upchirp waveform. A useful parameter is the instantaneous frequency, defined as
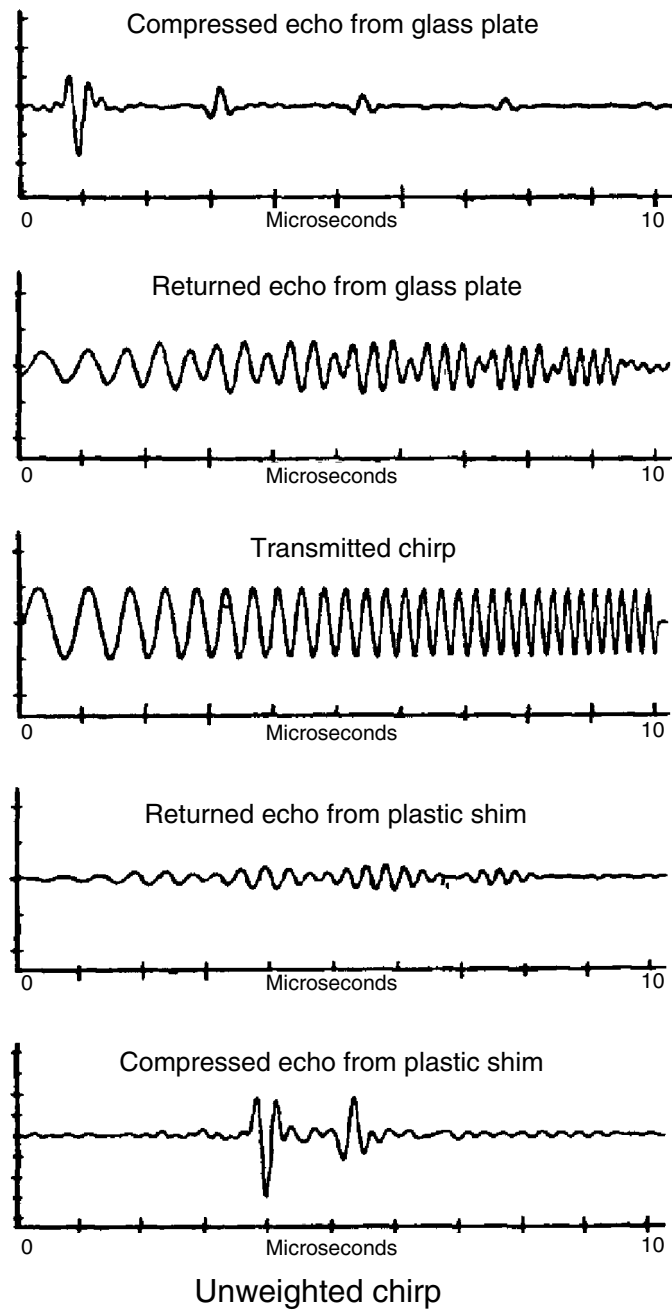
$$f_i = \left(\frac{1}{2\pi}\right)\frac{d\phi}{dt} \tag{10.6}$$

where ϕ is the phase of the analytic signal as a function of time (see Appendix A). For the transmit chirp of Figure 10.16, the instantaneous frequency as a function of time
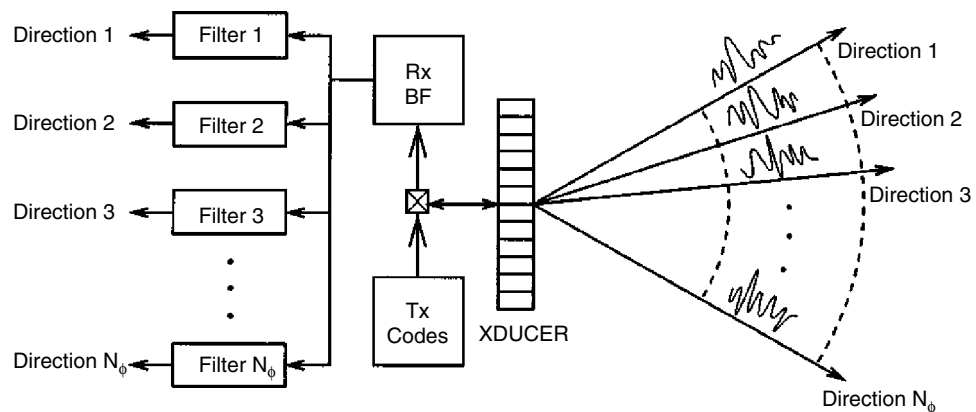
Figure 10.15 Simultaneous multibeam encoded ultrasound imaging system (from Shen and Ebbini, 1996, *IEEE*).

Compressed echo from glass plate

0   Microseconds   10

Returned echo from glass plate

0   Microseconds   10

Transmitted chirp

0   Microseconds   10

Returned echo from plastic shim

0   Microseconds   10

Compressed echo from plastic shim

0   Microseconds   10

Unweighted chirp

Figure 10.16   A chirp extending from 5 to 9 MHz (middle panel) and returned (uncompressed) and compressed pulse echoes from a glass plate and a plastic shim (from Lewis, 1987, *IEEE*).

is an ascending line from 5 to 9 MHz. The second panel from the top of Figure 10.16 shows the received echoes for a glass plate. After passing through the matched filter, these echoes are compressed to give excellent resolution and indicate multiple internal reflections into the top panel. A pair of similar echo signals for a plastic plate with higher internal absorption is shown in the lower two panels of Figure 10.16. The pros and cons of this methodology are discussed in the previous references. Both orthogonal codes and chirped waveform matched filters have been implemented on commercial systems.

10.10   BACK END

10.10.1   Scan Conversion and Display

The main function of the back end (refer to Figure 10.3, the block diagram) is to take the filtered RF vector line data and put it into a presentable form for display. These steps are the final ones in the process of imaging (described in detail in Section 8.4). An imaging challenge is to take the original large dynamic range, which may be originally on the order of 120 dB, and reduce it down to about 30 dB, which is the maximum gray-scale range that the eye–brain system can perceive. The limits and description of human visual perception is beyond the scope of this work, and they are described in more detail in Sharp (1993). As we have seen, the initial step is taken by the TGC amplifiers, which reduce the dynamic range to about 55–60 dB. The beam-formed digitized signals are converted to real (I) and quadrature (Q) components (delayed from the I signal by a quarter of the fundamental period). These components can be combined to obtain the analytic envelope of the signal through the operation $\sqrt{I^2 + Q^2}$.

In Figure 10.17, the envelope detection begins the back-end processing. This step is followed by an amplifier that can be controlled by the user to operate linearly at one extreme, or as a logarithmic amplifier at the other extreme, or as a blend between the two extremes to achieve further dynamic range compression. For example, in the case in which soft-tissue detail and bright specular targets coexist in the same image, the logarithmic characteristic of the amplifier can reduce the effects of the specular reflections on the high end of the scale. The preprocessing step, not done in all systems, slightly emphasizes weak signals as the number of bits is reduced, for example, from 10–7 bits after digitization.

So far, a number of vectors (lines with direction) have undergone detection, amplification, preprocessing (if any), and resampling to a certain number of points per line for suitable viewing. In order to make a television or PC-style rectangular image, this information has to be spatially remapped by a process called scan conversion. If the vectors were displayed in their correct spatial positions, the data would have missing information when overlaid on a rectangular grid corresponding to pixel locations in a standard raster scan, such as the NTSC TV. Sector scanning is one of the more challenging formats to convert to TV format (as illustrated by Figure 10.18). An enlargement of the polar coordinate scan lines overlaid on the raster rectangular pixel
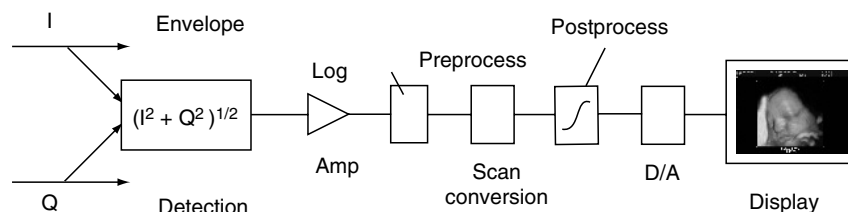
Figure 10.17   Block diagram for back-end processing used for image display (courtesy of Philips Medical Systems).

grid indicates the problem. Not only do the scan lines rarely intersect the pixel locations, but also each spatial position in the sector presents a different interpolation because the vectors change angle and are closer toward the apex of the sector. Early attempts at interpolation caused severe artifacts, such as Moire's pattern, and unnatural steps and blocks in the image. This problem can be solved by a 2D interpolation method (Leavitt *et al.*, 1983), which is shown in the bottom of Figure 10.18. The actual vector points are indicated along the bold scan lines with the pixel locations marked by crosses. To obtain the interpolation at a desired point (*Z*), first the radius from the apex to the intended pixel point is determined. Second, the angle of a radial line passing through *Z* is found. The generalized 2D interpolation formula is

$$Z(r, \theta) = \sum_n \sum_m S(r - n\Delta r, \theta - m\Delta\theta) \, Z(n\Delta r, m\Delta\theta) \qquad (10.7)$$

where *S* is a 2D triangular function.

The next step is one in which the amplitudes in the rectangular format undergo a nonlinear mapping called postprocessing. A number of postprocessing curves are selectable by the user to emphasize low- or high-amplitude echoes for the particular scan under view. This choice determines the final gray-scale mapping, which is usually displayed along with the picture. In some cases, pure B-mode images undergo an additional color mapping (sometimes called colorization) in order to increase the perceived dynamic range of values. Finally, a digital-to-analog (D/A) conversion occurs for displaying the converted information. The usual video controls such as brightness and contrast are also available, but they play a minor role compared to the extensive nonlinear mapping processes the data has undergone. Image plane overlays are used to present graphic and measurement information. Color flow display (to be covered in Chapter 11) also undergoes scan conversion and is displayed as an image plane overlaid on the gray-scale B-mode plane. In addition, most systems have the capability to store a sequence of frames in internal memory in real time for cine loop display.

10.10.2   Computation and Software

Software plays an indispensable and major role in organizing, managing, and controlling the information flow in an imaging system, as well as in responding to external
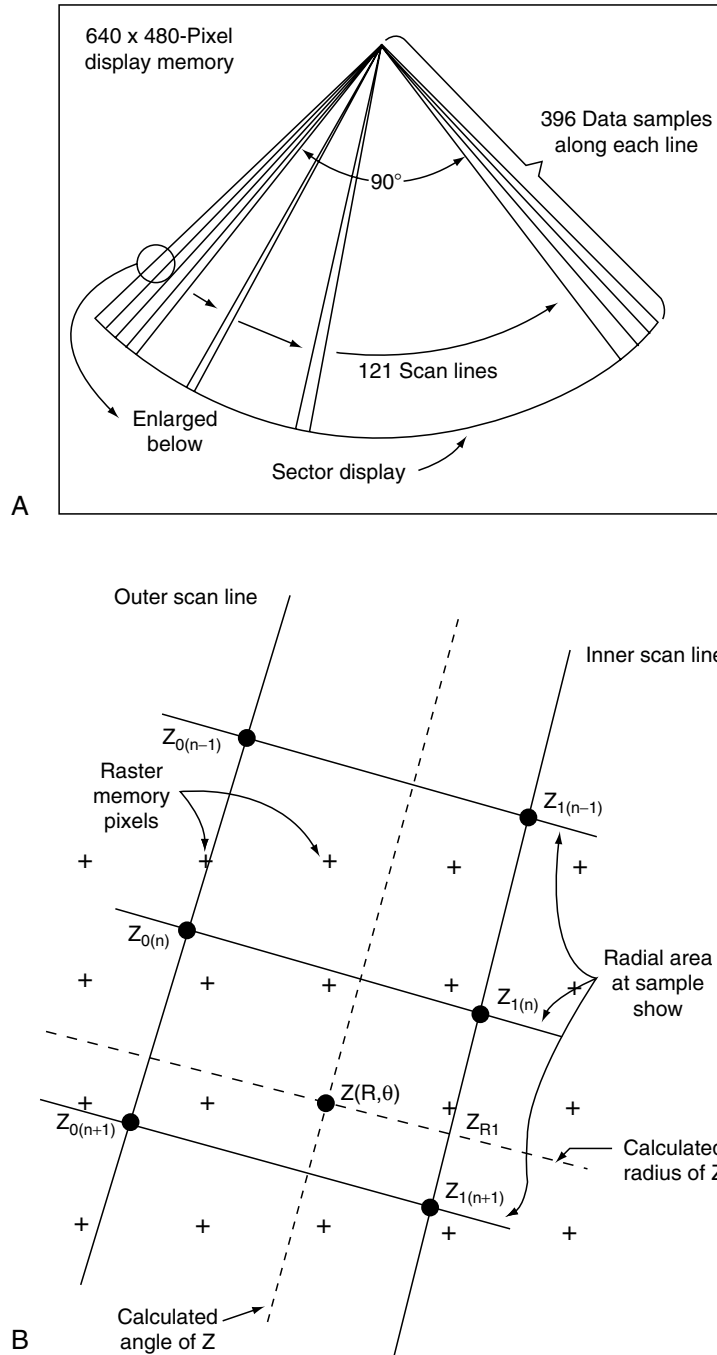
Figure 10.18 (A) Image vectors in a sector scan display overlaid on desired rectangle format. (B) Magnified view comparing vector data in polar coordinates to rectangular pixel positions (Reprinted by permission of Hewlett Packard, from Leavitt *et al.*, 1983, Hewlett Packard).

control changes or interrupts. First, it starts and stops a number of processes such as the transmit pulse sequence. Interrupts or external control changes by the user are sensed, and the appropriate change commands are issued. The master controller may have other slave microprocessors that manage specific functional groups, such as beamforming, image scan conversion and display, calculations and measurements of on-screen data, hardware, and digital signal processing (DSP) chips. The controller also manages external peripheral devices such as storage devices and printers as well as external communication formats for LAN and DICOM. The controller also supervises the real-time computation of parameters for the output display standard (to be described in Chapter 15), as well as acoustic output management and control.

## 10.11 ADVANCED SIGNAL PROCESSING

10.11.1 High-End Imaging Systems

The difference between a basic ultrasound imaging system and a high-end system is image quality. High-end systems employ advanced signal processing to achieve superior images. Acuson was the first to recognize that a "high-end" system could be successful in the clinical marketplace. The first Acuson images were known for their spatial resolution, contrast, and image uniformity (Maslak, 1985). Soon other manufacturers took up the challenge, and the striving for producing the best image continues today.

Three examples of advanced processing for enhancing image quality are attenuation compensation, frequency compounding, and spatial compounding (Schwartz, 1993). Usually separate signal processing paths and functions are combined in new ways to achieve improved images. In Figure 10.19 is a block diagram of an ultrasound imaging system; it has several differences from the block diagram of Figure 10.3. To the right of the transducer are scanner functions: beamforming and filtering. The remaining functions are back-end functions of image detection, logarithmic compression, and frame generation. At the bottom of the figure are a number of new blocks (numbered 1–4). Not all the steps of image information are included in this diagram, which is more symbolic and emphasizes differences in signal processing more than traditional imaging architectures. Controlling software to manage the interplay between different functions is assumed.

10.11.2 Attenuation and Diffraction Amplitude Compensation

TGC is an approach available to imaging system users to manually adjust for the changes in echo-amplitude caused by variations in beam-formation along the beam axis and by absorption. Better image improvements can be obtained by analyzing the video data and adaptively remapping the gain in an image in a 2D sense. At least two different approaches have appeared in literature (Melton and Skorton, 1981; Hughes and Duck, 1997). The first method senses differences in RF backscatter and adaptively changes TGC gains. The second analyzes each line of video data to read just the
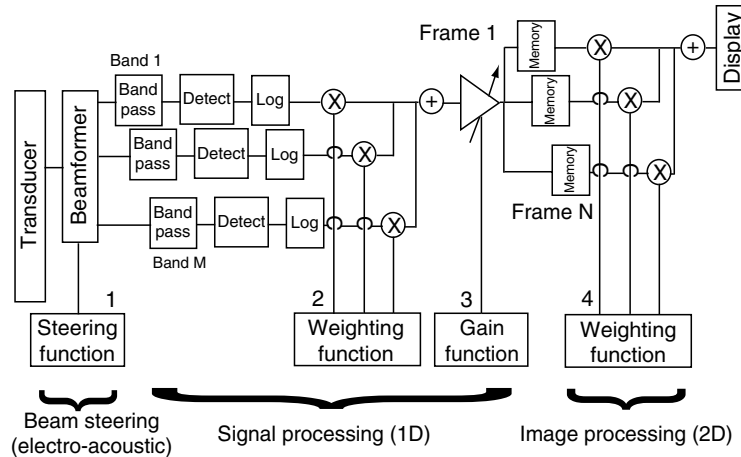
Figure 10.19 Imaging system architecture with signal processing enhancements. The lower blocks are numbered as (1) steering function, (2) spectral weighting function, (3) gain function, and (4) weighting function (courtesy of G. A. Schwartz, Philips Medical Systems).

intensity levels as a function of time, based on an algorithm, and it leads to an image renormalized at each spatial point. This last approach is more suitable for imaging systems because it can be accomplished in software without major hardware changes.

Using this method as an example, we return to Figure 10.19, block 3 (gain function). The triangle above it symbolizes a variable gain control. A line of video data, corrected for previous video processing and TGC settings, passes through the amplifier and is sent down to the gain control or video analyzer software (not shown in diagram). This line of data is analyzed by an adaptive attenuation estimation algorithm, and the renormalization factor or new gain is determined for each time sample and is sent back through the adjusted amplifier. Only the renormalized values of video information pass through the normal digital scan conversion process (not shown) to create a compensated image frame that is stored in frame memory.

10.11.3 Frequency Compounding

The concept of frequency diversity to reduce speckle was discussed in Section 8.4.6. Until the 1980s, some clinicians valued the grainy texture of speckle, believing it to contain tissue information. In Chapter 8, speckle was shown to be mainly artifactual. Images of the same tissue taken by different transducers at various frequencies present different-looking speckle. Researchers have shown (Abbot, 1979; Melton and Magnin, 1984; Trahey *et al*.,1986) the benefits of smoothing out speckle through a scheme of subdividing the pulse-echo spectrum into smaller bandwidths and then recombining them. Through frequency diversity, improved contrast is obtained and more subtle gradations in tissue structure can be distinguished.
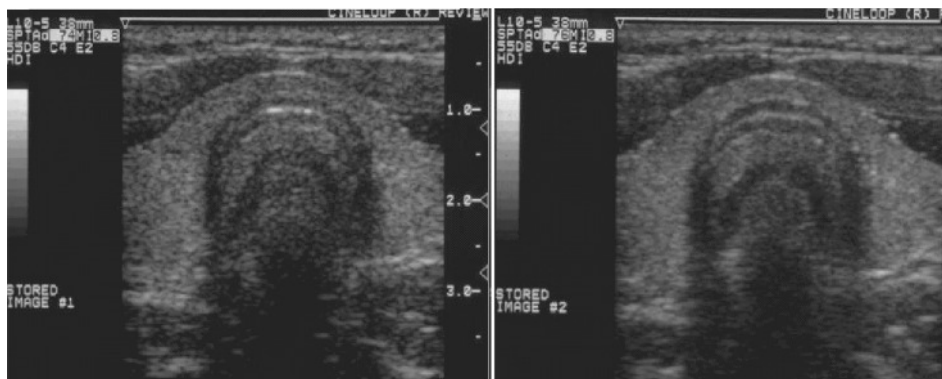
Figure 10.20 (Left) Conventional imaging. (Right) Frequency compounding (courtesy of G. A. Schwartz, Philips Medical Systems).

A way in which frequency compounding can be implemented is illustrated by Figure 10.19. RF data from a summed beamformed line are sent in parallel to a number (M) of bandpass filters and detection. Each detected signal path is assigned a weight according to a spectral weighting function (block 2) and summed to form a final composite line for scan conversion. Because speckle depends on the constructive and destructive interference at a particular frequency, this 1D summing process reduces the variance of the speckle. Clinical images with and without frequency compounding are compared in Figure 10.20.
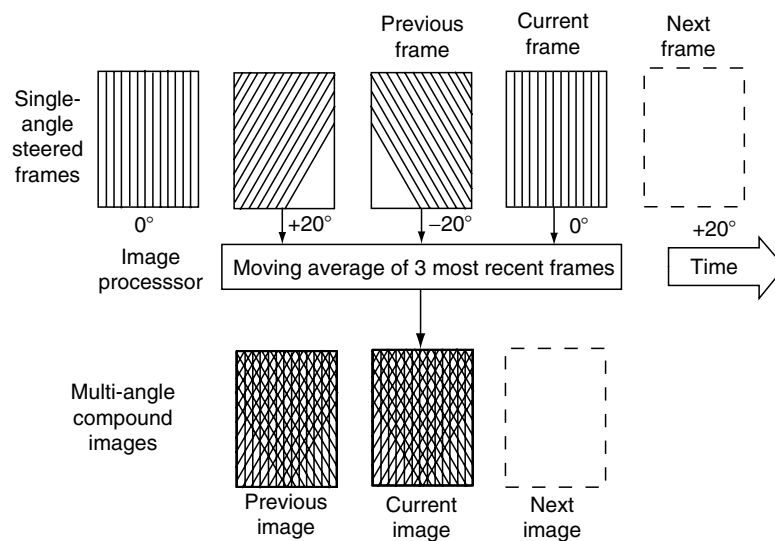
10.11.4 Spatial Compounding

While spatial diversity was also named as a way of reducing speckle in Section 8.4.6, there is a more important reason for using it—new backscattering information is introduced into an image. Artifacts are usually thought of as echo features that do not correspond to a real target or the absence of a target. A more subtle artifact is a distortion or a partial depiction of an object. Obvious examples are echoes from a specular reflector, that are strongly angle dependent (as covered by Section 8.4.2). In that section, three angular views of a cylinder were shown in Figure 8.11. That cylinder is revisited in Figure 10.21 (once as seen by conventional imaging and also as seen by compound imaging). When viewed on a decibel scale, there is considerably more echo information available for the cylinder viewed from wider angles.

The implementation of real-time spatial compounding involves 1D and 2D processing. To generate a number (N) of different looks at an object, translation and rotation operations are combined in an array (as explained in Section 10.7). To acquire the necessary views efficiently, in addition to the normal (zero-degree) line orientation frame, N-1 single steered frames are also taken (as in Figure 10.6). A scheme for accomplishing compounding in real time is depicted in Figure 10.22. The moving average of N frames create each spatial compound frame. In the overall block diagram of Figure 10.19, a sequence of N steered angles is entered through
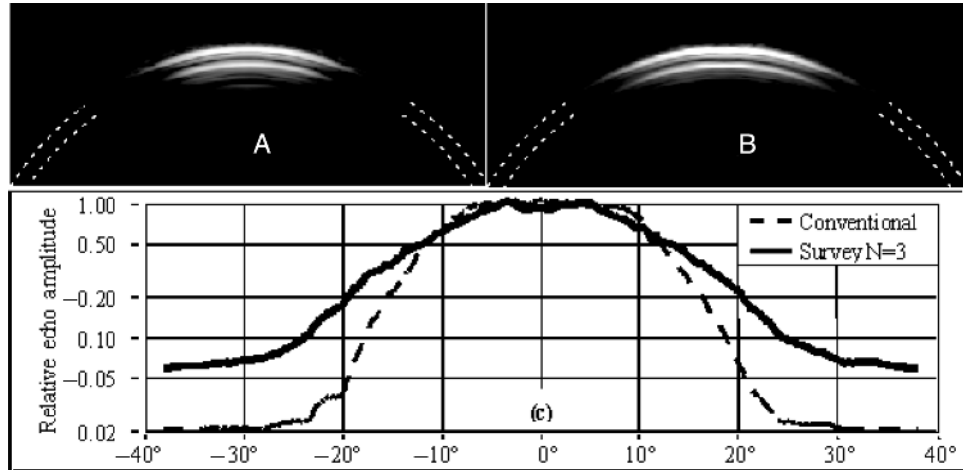
Figure 10.21   Specular reflection from a cylindrical reflector for (A) conventional and (B) compound imaging for steering angles of 17°, 0°, and −17°. (C) Corresponding echo amplitudes received by a 5–12 MHz linear array are plotted as a function of angular position (courtesy of Entrekin *et al.*, 2000, reprinted with permission of Kluwer Academic/Plenum Publishers).

Figure 10.22   Steps of real-time spatial compounding. In a sequence of steered frames, the scan-converted frames are combined with a temporal moving average filter to form compound images (courtesy of Entrekin *et al.*, 2000, reprinted with permission of Kluwer Academic/Plenum Publishers).

Figure 10.23 (A) Conventional and (B) compound views of an ulcerated carotid artery plaque as viewed with a 5–12 MHz linear array (courtesy of Entrekin *et al.*, 2000, reprinted with permission of Kluwer Academic/Plenum Publishers).

block 1. The *N*-scan-converted single-angle steered frames arrive in the back end where, according to a prescribed spatial compounding function of block 4, each frame *N* is assigned line and overall 2D frame weighting. Finally, the weighted frames are combined in an averaging operation (symbolized by the summing operation) before display.

Enhanced lesion detection, or the increase in contrast between a cyst and its surrounding material, as well as speckle signal-to-noise have been demonstrated for real-time spatial compounding (Entrekin *et al.*, 2000). Even though the views are not totally independent, these improvements follow a $\sqrt{N}$ trend. Figure 10.23 compares conventional and spatially compounded images of ulcerated plaque in a carotid artery. Enhanced tissue differentiation, contrast resolution, tissue boundary delineation, and the definition of anechoic regions are more evident in the spatially compounded image. One drawback of this method is that temporal averaging may result in the blurring of fast-moving objects in the field of view. This effect can be reduced by decreasing the number of frames (*N*) averaged; appropriate numbers have been determined for different clinical applications (Entrekin *et al.*, 2000).

10.11.5 Real-Time Border Detection

In order to determine the fast-moving changes of the left ventricle of the heart, a 2D signal processing method has been developed to track the endocardial border. This approach is based on automatically detecting the difference between the integrated backscatter of blood and the myocardium (heart muscle) (Loomis *et al.*, 1990; Perez *et al.*, 1991) at each spatial location. Implementation of this approach combines a blood–tissue discriminator filter and an algorithm for incoming pulse echoes with 2D signal processing to present a real-time display of the blood–tissue border. This border can be used for real-time calculations of related cardiac parameters.

Another cardiac problem of interest is akinetic motion of the heart due to injury, disease, or insufficient arterial blood supplies. The net effect is that the heart wall of the left ventricle no longer contracts and expands uniformly during the cardiac cycle,

and some local regions lag behind. The border-tracking algorithm described earlier can be applied to this problem. The change in border position from the previous frame is determined, and this change is assigned a unique color. From frame to frame, during either a contraction or expansion phase, the sequence of color changes are added to each other to paint an overall picture of wall motion (as depicted in Figure 10.24a). This ideal picture shows that borders have uniform thickness during a normal contracting cycle; tracking is synchronized with the electrocardiogram (ECG). In real time, this process has been used to track the walls of the left ventricle (shown in Figure 10.24b). Locally nonuniform expansion and contraction of the chamber can be detected from irregularities in the color patterns.

10.11.6   Three- and Four-Dimensional Imaging

One of the drawbacks of 2D ultrasound imaging is the skill and experience required to obtain good images and to make a diagnosis. Imaging in this way is demanding in terms of keeping track of the spatial relationships in the anatomy, and part of using this skill is being able to do 3D visualization in one's head during an exam. An ultrasound exam does not consist of just picture-perfect images such as those in this chapter. Instead, pictures are selected from a highly interactive searching process, during which many image planes are scanned in real time.

The primary goal of 3D ultrasound imaging is the user-friendly presentation of volume anatomical information with real-time interactive capabilities. This goal is challenging in terms of the acquisition time required, the amount of data processed, and the means to visualize and interact with the data in a diagnostically useful and convenient way. Image interpretation becomes simpler because the correct spatial relationships of organs within a volume are more intuitively obvious and complete, thereby facilitating diagnosis, especially of abnormal anatomy such as congenital defects and of distortions caused by disease. The probability of finding an anomaly has the potential of being higher with 3D than with manual 2D scanning because the conventional process may miss an important region or not present sufficient information for interpretation and diagnosis.

The process of 3D imaging involves three steps: acquisition, volume rendering, and visualization. For more details, excellent reviews of 3D imaging by Nelson and Pretorius (1998) and Fenster and Downey (1996) are recommended.

Acquisition is a throwback to the days of mechanical scanning discussed in Chapter 1, except with arrays substituted for single-element transducers. At any instant of time, the array is busy creating a scan plane of imaging data; however, in order to cover a volume, it is also mechanically scanned either through translation, rotation, or fanning. A major difference for 3D imaging is that position data must be provided for each image plane. As in the early mechanical scanning days, this information is provided by either built-in (or built-on) position sensors or by internal/external position controllers, by which the spatial location and or orientation of the array is changed in a prescribed way. The built-on sensors allow freehand scanning. Because acquisition time is on the order of seconds, data are often synchronized to the ECG, M-mode, or Doppler signals, so that, for example, enough frames are acquired at the
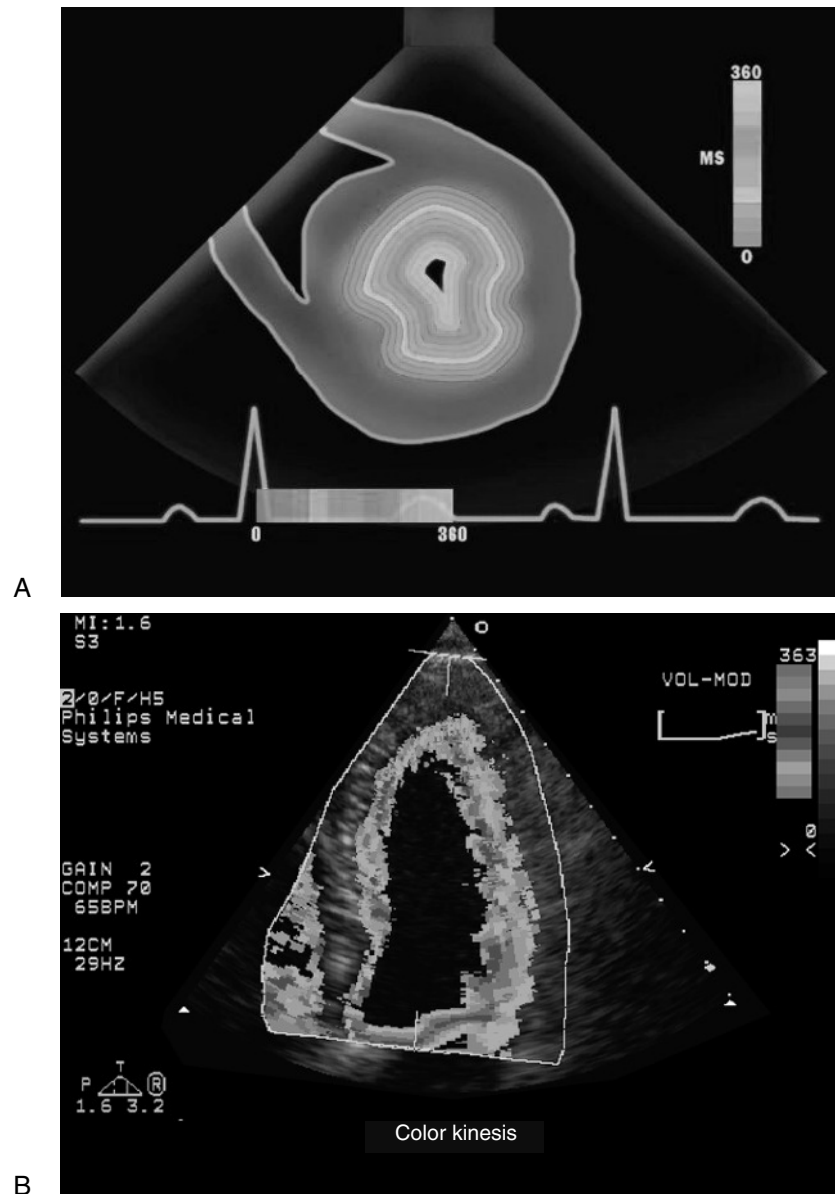
Figure 10.24   (A) Artist's depiction of color-kinesis automatic border-tracking algorithm, showing uniform contraction and synchronization to ECG. (B) Algorithm in operation shows severe akinetic behavior near the bottom of a left ventricle. Note the lack of motion near the base of the septal wall (lower left) and large motion on the opposite side of the chamber (lower right) (courtesy of Philips Medical Systems) (see also color insert).

same point in a cardiac cycle to create a volume. To create 4D images, time as well as position information is necessary for each acquired image plane. A recent innovation is the real-time 2D array, for which a volume of data can be acquired rapidly and completely electronically without moving the array.

The next step of the 3D process is that the video data in the image planes are interpolated into a volume of data in their correct spatial position. The 3D counterpart to pixels in 2D imaging is the voxel. Adequate sampling is important because a considerable amount of interpolation is involved. The quality of individual image planes is reflected in the final 3D images so that speckle, unequal resolution throughout the field of view, signal-to-noise, and patient movement are important. In this regard, a 2D array, in which the elevation and azimuth focusing are collocated, contributes to more resolution uniformity.

The visualization software takes the volume data and presents it in an interactive way for imaging. This step presents a challenge for some ultrasound data from soft tissues that do not have enough contrast for definitive segmentation. Slice presentation is the simultaneous display of several image planes that can be selected interactively from arbitrary locations and orientations within the volume. These slices are also referred to as multiplanar reformatting (MPR) views. Recently, techniques have been created for directly viewing the 3D matrix of echo signals. Such techniques are referred to as "volume rendering," and they produce surfacelike images of the internal anatomy. Although similar in presentation, such techniques should be distinguished from the more common surface-rendering techniques, which are used in computer animations and games and motion pictures. The most popular images of this kind are those of the fetus (see Figure 1.12), in which it is easier to distinguish between the fetal body and the surrounding amniotic fluid. Volume rendering is also applicable to functional information; for example, one can use color flow 4D imaging to visualize both normal and pathologic flows in 3D space. Ease of use of the interactive visualization software is an ongoing concern and focus of development.

A more recent change in visualization capability is the introduction of a real-time 2D array by Philips Medical Systems (see Section 7.9.2). This array has the equivalent of combined front-end and micro-beamforming functions in the handle of the transducer. Electronic 3D scanning in real time provides rapid acquisition of volume data and simultaneous viewing of different image planes as well. A frame from a real-time 4D sequence of the opening and closing of heart valves is shown in Figure 10.25.

10.12   ALTERNATE IMAGING SYSTEM ARCHITECTURES

This chapter completes the central block diagram of Figure 2.14. Blocks *F* (for filtering), *D* (for detection), and *D* (for display) provide the last pieces of the imaging system. The overall structure in this diagram (the linear phased array architecture), borrowed from electromagnetic array antennas, has had a surprisingly long run. This type of beamformer is straightforward to implement, real time, simple, and robust, and it has high angular selectivity. No contenders have been demonstrated to be

Figure 10.25 Real-time 4D image frame of heart valve motion (courtesy of Philips Medical Systems).

improvements over the original architecture in a clinical setting. The present beam-former has two chief limitations: lack of speed and flexibility.

An example of the flexibility issue is its inability to handle aberration well. This last problem has been addressed by several schemes (as discussed in Chapter 9). Adaptive imaging systems for this purpose were described by Krishnan *et al*. (1997) and Rigby *et al*. (2000). Another adaptive scheme for minimizing the effects of off-axis scatterers was described by Mann and Walker (2002). A scheme for extracting more angular backscattering information for imaging was presented by Walker and McAllister (2002).

In terms of improving speed, novel methods have been proposed (von Ramm *et al*., 1991). The key limitation in conventional systems is the pulse-echo round-trip time that adds up, line by line. Several alternative methods employ broad transmit beams to overcome the long wait for images. Lu (1997, 1998) has devised a very fast frame-rate system based on a plane wave transmission, X-receive beams, and a Fourier transform technique. A new company, Zonare, has been formed based on an architecture that includes the transmission of several (approximately 10) broad plane wave-beams per frame and fast acquisition and signal processing (Jedrzejewicz *et al*., 2003). Jensen and his colleagues at the University of Copenhagen have developed a fast synthetic aperture system that includes broad-beam transmit insonification. They provide a discussion of other limitations of conventional imaging, such as fixed transmit focus-

ing (Jensen *et al.*, 2002). These systems have the potential for more than just speed; they may be able to acquire more complete information-laden data sets, as well as have time to provide more sophisticated and tissue-appropriate processing and to extract relevant parameters for diagnostic imaging.

BIBLIOGRAPHY

Foster, F. S., Larson, J. D., Mason, M. K., Shoup, T. S., Nelson, G., and Yoshida, H. (1989a). Development of a 12 element annular array transducer for realtime ultrasound imaging. *Ultrasound in Med. & Biol.* **15**, 649–659. Details the design of an annular array digital imaging system.

Foster, F. S., Larson, J. D., Pittaro, R. J., Corl, P. D., Greenstein, A. P., and Lum, P. K. (1989b). A digital annular array prototype scanner for realtime ultrasound imaging. *Ultrasound in Med. & Biol.* **15**, 661–672. Another article detailing the design of an annular array digital imaging system.

Hewlett Packard Journal **10**, Vol. 34. (Oct. 1983). Describes the operation of HP's first generation of imaging systems in detail.

Hewlett Packard Journal **12**, Vol. 34. (Dec. 1983). A special issue that continues the description in the above reference.

Kino, G. S. (1987). *Acoustic Waves: Devices, Imaging, and Analog Signal Processing*. Prentice-Hall, Englewood Cliffs, NJ. Provides acoustic imaging theory and applications available on CD-ROM from IEEE-UFFC Group.

Kremkau, F. W. ( ). *Diagnostic Ultrasound: Principles and Instruments*. This introductory book investigates the topic of imaging systems in more depth. It has a wealth of information that is clearly presented at an easily understood level.

Morgan, D. P. (1991). *Surface Wave Devices*. (Available on CD-ROM from IEEE-UFFC Group.) Ferroelec and Freq. Control Society. Additional information about signal processing, encoding, and chirped waveforms for an allied field and surface acoustic wave devices.

REFERENCES

Bracewell, R. (2000). *The Fourier Transform and Its Applications*, Chap. 17. McGraw Hill, New York.

Carr, P. H., DeVito, P. A., and Szabo, T. L. (1972). The effect of temperature and Doppler shift on the performance of elastic surface wave encoders and decoders. *IEEE Trans. Sonics Ultrason.* **SU-19**, 357–367.

Chiao, R. Y. and Hao, X. (2003). Coded excitation for diagnostic ultrasound: A system developer's perspective. *Ultrason. Symp. Proc.*, 437–448.

Chiao, R. Y., Thomas, L. J., and Silverstein, S. D. (1997). Sparse array imaging with spatially-encoded transmits. *IEEE Ultrason. Symp. Proc.*, 1679–1682.

Cole, C. R. (1991). Properties of swept FM waveforms in medical ultrasound imaging. *IEEE Ultrason. Symp. Proc.*, 1243–1248.

Entrekin, R. R., Jago, J. R., and Kofoed, S. C. (2000). Real-time spatial compound imaging: Technical performance in vascular applications. *Acoustical Imaging*, Vol. 25. Halliwell, M. and Wells, P. N. T. (eds.). Kluwer Academic/Plenum Publishers, New York, pp. 331–342.

Fenster, A. and Downey, D. B. (1996). 3-D ultrasound imaging: A review. *IEEE Eng. Med. Bio.* **15**, 41–49.

Foster, F. S., Larson, J. D., Mason, M. K., Shoup, T. S., Nelson, G., and Yoshida, H. (1989a). Development of a 12 element annular array transducer for realtime ultrasound imaging. *Ultrasound in Med. & Biol.* **15**, 649–659.

Foster, F. S., Larson, J. D., Pittaro, R. J., Corl, P. D., Greenstein, A. P., and Lum, P. K. (1989b). A digital annular array prototype scanner for realtime ultrasound imaging. *Ultrasound in Med. & Biol.* **15**: 661–672.

Genis V., Obeznenko, I., Reid, I. M., and Lewin, P. (1991). Swept frequency technique for classification of the scatter structure. *Proc. of Annual Conf. on Engineering in Med. and Biol.* 13: 167–168.

Hughes, D. I. and Duck, F. A. (1997). Automatic attenuation compensation for ultrasonic imaging. *Ultrasound in Med. & Biol.* **23**, 651–664.

Jedrzejewicz, T., McLaughlin, G., Napolitano, D., Mo, L., and Sandstrom, K. (2003). Zone acquisition imaging as an alternative to line-by-line acquisition imaging. *Ultrasound in Med. & Biol.* **29**, No. 5S, S69–70.

Jensen, J. A., Nikolov, S. I., Misaridis, T., and Gammelmark, K. L. (2002). Equipment and methods for synthetic aperture anatomic and flow imaging. *Ultrason. Symp. Proc.*, 1518–1527.

Kino, G. S. (1987). *Acoustic Waves: Devices, Imaging, and Analog Signal Processing*. Prentice-Hall, Englewood Cliffs, NJ.

Krishnan, S., Rigby, K. W., and O'Donnell, M. (1997). Adaptive aberration correction of abdominal images using PARCA. *Ultrason. Imag.* **19**, 169–179.

Leavitt, S. C., Hunt, B. F., and Larsen, H. G. (1983). A scan conversion algorithm for displaying ultrasound images. Hewlett Packard J. **10**, Vol. 34., 30–34.

Lee, B. B., and Ferguson, E. A. (1982). Golay codes for simultaneous multi-mode operation in phased arrays. *IEEE Ultrason. Symp. Proc.*, 821–825.

Lewis, G. K. (1987). Chirped PVDF transducers for medical ultrasound imaging. *IEEE Ultrason. Symp. Proc.*, 879–884.

Lu, J.-yu. (1997). 2D and 3D high frame rate imaging with limited diffraction beams. *IEEE Trans. Ultrason. Ferroelec. Freq. Control* **14**, 839–856.

Lu, J-yu. (1998). Experimental study of high frame rate imaging with limited diffraction beams. *IEEE Trans. Ultrason. Ferroelec. Freq. Control* **45**, 84–97.

Mann, J. A., and Walker, W. F. (2002). A constrained adaptive beamformer for medical ultrasound: Initial results. *IEEE Ultrason. Symp. Proc.*, 1763–1766.

Maslak, S. M. (1985). Computed sonography. *Ultrasound Annual 1985*. R. C. Sanders and M. C. Hill (eds.). Raven Press, New York.

Melton Jr., H. E. and Skorton, D. J. (1981). Rational-gain-compensation for attenuation in ultrasonic cardiac imaging. *Ultrason. Symp. Proc.*, 607–611.

Morgan, D. P. (1991). *Surface Wave Devices*. For signal processing Elsevier, Amsterdam.

Nelson, T. R. and Pretorius, D. H. (1998). Three-Dimensional ultrasound imaging. *Ultrasound in Med. & Biol.* **24**, 1243–1270.

O'Donnell, M. (1992). Coded excitation system for improving the penetration of real time phased-array imaging systems. *IEEE Trans. Ultrason. Ferroelec. Freq. Cont.* **39**, 341–351.

Perez, J. E., Waggoner, A. D., Barzilia, B., Melton, H. E., Miller, I. G., and Soben, B. E. (1991). New edge detection algorithm facilitates two-dimensional echo cardiographic on-line analysis of left ventricular (LV) performance J. Am. Coll. Cardiol. 17: 291A.

Rigby, K. W., Chalek, C. L., Haider, B., Lewandowski, R. S., O'Donnell, M., Smith, L. S., and Wildes, D. S. (2000). In vivo abdominal image quality using real-time estimation and correction of aberration. *IEEE Ultrason. Symp. Proc.*, 1603–1606

Schwartz, G. S. (2001). Artifact reduction in medical ultrasound. *J. Acoust. Soc. Am.* **109**, 2360.

Sharp, P. F. (1993). *Advances in Ultrasound Techniques and Instrumentation*, Chap. 1. P. N. T. Wells (ed.). Churchill Livingstone, New York.

Shen, J. and Ebbini, E. S. (1996a). A new coded-excitation ultrasound imaging system, Part I: Basic principles. *IEEE Trans. Ultrason. Ferroelec. Freq. Control* **43**, 141–148.

Shen, J. and Ebbini, E.S. (1996b). A new coded-excitation ultrasound imaging system, Part II: Operator design. *IEEE Trans. Ultrason. Ferroelec. Freq. Control* **43**, 131–140.

Shoup, T. A. and Hart, J. (1988). Ultrasonic imaging systems. *Ultrason. Symp. Proc.*, 863–871.

Szabo, T. L., Melton Jr., H. E., and Hempstead, P. S. (1988). Ultrasonic output measurements of multiple mode diagnostic ultrasound systems. *IEEE Trans. Ultrason. Ferroelec. Freq. Control* **35**, 220–231.

Tirumalai, A. P., Lowery, C., Gustafson, G., Sutcliffe, P., and von Behren, P. (2000). Extended-field-of-view ultrasound imaging. *Handbook of Medical Imaging*, Vol. 3: Display and PACs. Y. Kim and S. C. Horii (eds.). SPIE Press Vol. PM81.

von Ramm, O.T., Smith, S. W., and Pavy Jr., H. E. (1991). High-speed ultrasound volumetric imaging system, Part II: Parallel processing and image display. *IEEE Trans. Ultrason. Ferroelec. Freq. Control* **38**, No. 2, 109–115.

Walker, W. F. and McAllister, M. J. (2002). Angular scatter imaging: Clinical results and novel processing. *IEEE Ultrason. Symp. Proc.*, 1528–1532.

Wells, P. N. T. (1993). *Advances in Ultrasound Techniques and Instrumentation*. Churchill Livingstone, New York.